Nanomed J. 11(4): 458-467, Autumn 2024

RESEARCH PAPER

Electrochemical investigation of dopamine and hydroquinone by (Pd@Au-PANI) nanocomposite

Zaid H. Mahmoud [1]*, H. N. K. AL-Salman [2], Maha Khalid Abdulameer [3], Russul Reidh Abass [4], Tholfiqar Najah Ismael [5], Dheyaa Yahaia Alhameedi [6], Mahmood Hasen Shuhata Alubiady [7], Ahmed Muzahem Al-Ani [8], Sally Salih Jumaa [9]

[1]Chemistry department, college of sciences, university of Diyala
[2]Department of Pharmaceutical Chemistry, College of Pharmacy, University of Basrah, Basrah, Iraq
[3]Department of Radiology & Sonar Techniques, Al-Noor University College, Nineveh, Iraq
[4]Medical Lab. Techniques Department, College of medical Technology, Al-Farahidi University, Baghdad,Iraq
[5]Department of Medical Instrumentation Engineering Techniques/ Imam Jaafar Al-Sadiq University/Iraq
[6]Department of Anesthesia, College of health & medical Technology, Sawa University, Almuthana, Iraq
[7]Department of Medical Engineering, Al-Hadi University College, Baghdad,10011, Iraq
[8]Department of Medical Engineering, Al-Nisour University College, Baghdad, Iraq
[9]Department of Medical Engineering, National University of Science and Technology, Dhi Qar, Iraq

ABSTRACT

Objective(s): Electrochemical estimation of dopamine by synthesized Pd@Au-PANI nanocomposite.
Materials and Methods: Au-doped and Au-Pd incorporated PANI nanocomposites were prepared via oxidative polymerization and hydrothermal methods with ammonium persulphate.
Results: As-suggested biosensor was improved for the simultaneous disclosure of dopamine and hydroquinone, displayed low detection limits of 0.46 µM for dopamine and 0.23 mM for hydroquinone.
Conclusion: The fabricated biosensor showed broad linear ranges for dopamine (5-25 µM), and hydroquinone (0.5-2.5 mM). Along with these good results, the Au-Pd@PANI nanotube also implemented good stability and reproducibility.

Keywords: *Biosensor, Bimetallic, Cyclic voltammetry, Differential pulse voltammetry, Nanotube*

How to cite this article
H Mahmoud Z, K. AL-Salman HN, Khalid Abdulameer M, Reidh Abass R, Najah Ismael T, Yahaia Alhameedi D, Hasen Shuhata Alubiady H, Muzahem Al-Ani M, Salih Jumaa S. Electrochemical investigation of dopamine and hydroquinone by (Pd@Au-PANI) nanocomposite . Nanomed J. 2024; 11(4): 458-467. DOI: 10.22038/nmj.2024.78083.1906

INTRODUCTION

Dopamine (DA) and hydroquinone (HQ) are two popular materials with considerable biomedical applications [1]. HQ is a ubiquitous phenolic compound with good redox properties [2], poisonous considerable environmental and health hazard because of its low biodegradability and high toxicity [3]. Its expansion in pharmaceuticals, cosmetics, and human diet exacerbates ecological defilement and human health dangerous [4]. Regulatory proxies like EU and EPA have identified HQ as a main pollutant, as well as, China has determined its permitted level as 0.5 mg/mL. On the medical side, DA as a transfer neurotransmitter participates in many biological processes, such as perception and passion. Abnormal DA levels are for the reason of many diseases, like anorexia and schizophrenia [5]. Given that premature disclosure can mainly enhance treatment results, and there is an imperative requirement of selective methods for controlling or monitoring DA levels. So, the accurate and credible detection of DA and HQ is important for clinical characterization and ecological safety. Until now, many characterization and analytical techniques have been evolved for quantification of DA and HQ, such as HPLC [6], GC [7], and fluorescence [8]. Electrochemical techniques give prompt response, simplicity, good results, and low cost, making them typical for budget-friendly and portable implementations [9]. However, the pres-

* *Corresponding author: Email: zaidhameed_91@yahoo.com*
Note. This manuscript was submitted on February 11, 2024; approved on April 2, 2024

ent reports lack the proof of simultaneous electrochemical disclosure for DA and HQ. The choose of appropriate electrode modifiers is compulsory for electroanalytical determination of analytes. The system of bimetallic is anticipated to appear not only the features combination of two metals, but also new properties due to the synergy impact between different metals [10]. The synergistic impact of bimetallic compound can appear more activity compared to monometallic even at low concentration. Many bimetallics such as Au-Pt [11], Au-Ag [12] and Pd/Au [13] have been reported as heterogeneous catalysts. It has been announced that the activity of a bimetallic is fundamentally connected to the dispersion and size. The low range of particle size of a bimetallic with excellent dispersion is a good choice for great catalytic activity because of its high surface to volume ratio [14]. However, the nanoparticles have a penchant to agglomerate through their electrolytic applications due to high surface energy, which can border their activity [15-29]. Thereby, the variuos compounds can be used to stabilize these effective compounds, such as carbon nanotubes and polymers [30]. Among most polymer-based materials, particularly polyanilne nanotubes (PANI) with intrinsic carrier mobility, excellent surface area, and ecological stability are so critical to exterior interference electric field in disclosure process of electric field [31-33]. PANI nanotube-based sensors provide good response and excellent selectivity. On the other side, bimetallic nanocomposite has been vastly studied among other metal nanoparticles [34]. Guo et al. used ion exchange method to prepare good structured (Co-Ni) OH for energy applications [35]; while Song et al. designed a Co-Ni based carbonates via optimizing Co/Ni atomic ratio, which illustrated excellent rate execution in asymmetrical solid-state supercapacitors [36]. Liao et al. reported using rGO/Ni@Co in electrochemical sensor application for determining DA [37]. These studies appeared the bimetallic composites potential in electrochemical sensing. In this study, a bimetallic Au-Pd@PANI nanocomposite was synthesized utilizing co-precipitation and hydrothermal methods and performed for electrochemical investigations. Au-Pd@PANI nanocomposite is anticipated to able simultaneous disclosure of DA and HQ with improved sensitivity.

Experimental section

Materials

All chemicals were supplied from Merck Co., analytical grade and utilized without future purification.

Synthesis of PANI nanotube

First, 3 mL of aniline monomer and 20 mL of hydrochloric acid (1M) were mixed and stirred in ice bath. Then, 10 mL of ammonium peroxydisulfate (APS, 1M) was dripped to the mixture with high stirring for 4 hr at 0 °C. Then, the black-green suspension was transferred to 250 mL autoclaves for hydrothermal reaction at 180 °C for 2 hr. Finally, the formed precipitate was filtered, washed and dried at 70 °C for 3 hr.

Synthesis of Au-Pd@PANI tubes

Briefly, 0.5 g of PANI was dispersed in 50 mL absolute ethanol ultrasonically for 30 min. After that, 0.5 g of palladium chloride and 0.2 g of tetrachloroauric(III) acid, and trihydrateand hydrazine (10 mL) were added to pretreated PANI and 100 mL distilled water in a 200 mL round. Then, the mixture was refluxed for 3 h at 80 °C. The formed precipitate was isolated and washed by acetone and distilled water, followed via drying at 70 °C for 5 hr. Full procedure is shown in Fig. 1.

Electrochemical measurement

In this study, a standard three-electrode system contained Ag/AgCl (saturated KCl), Pt wire, and modified glassy carbon as counter, reference, and working electrodes, respectively, Phosphate buffer solution (0.1 M, pH 7) was used as electrolyte solution. The electroanalytical measurements were carried out by using cyclic voltammetry within range of -0.2-0.8 mV and scan rate of 30 mV/s, and differential pulse voltammetry employed with the voltage step of 5 mV. Before all experimental, the electrochemical cell was injected by N_2 gas to purge O_2 gas, which allowed standard curves generation depended on the different signal responses for the concentrations of DA and HQ.

RESULTS AND DISCUSSIONS

Bimetallic nanoparticle characterization

The UV-Vis spectra of PANI, Au, Pd-Au,

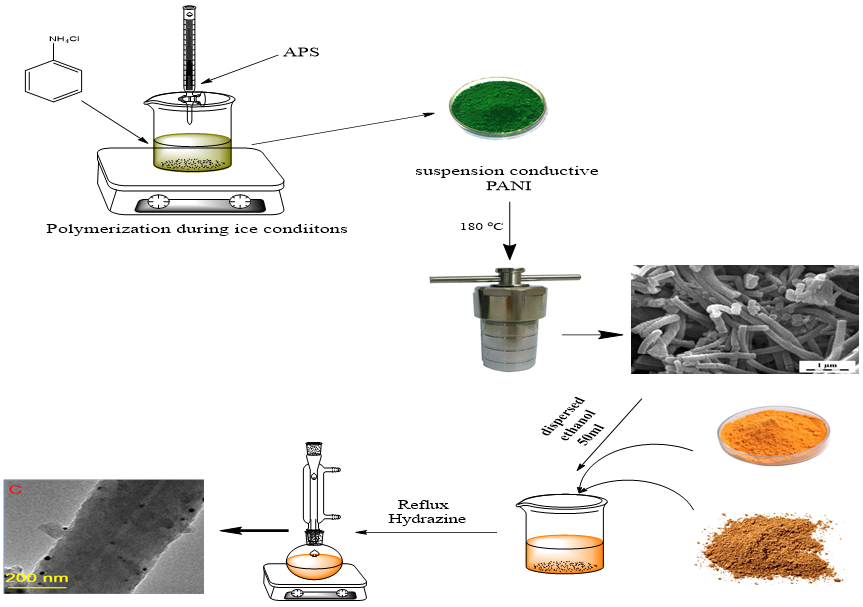

Fig. 1 Producer for synthesis of Au-Pd@PANI nanotubes

Au-PANI, and Au-Pd/PANI nanocomposite are shown in Fig. 2A. The results shown the Plasmon resonance peak for Au nanoparticles and a broad peak as a shoulder for the production of Au-Pd nanoparticles at 535 nm. PANI, Au/PANI, and Au-Pd/PANI nanocomposite appeared two absorption peaks locating at 355 and 625 nm, attributed to * and n-* of benzenoid and quinonid ring transitions of PANI, respectively. On the other handa reduce in peak intensity after incorporating with PANI was assigned to doping Au and Au/Pd in PANI matrix. The FT-IR spectra of pure Au, Au- doped PANI, and Au/Pd-doped PANI

are displayed in Fig. 3B. The results demonstrate that the peaks located at 1620, 1480, and 1495 cm^{-1} are assigned to C-C stretching vibration of quinonoid and benzenoid rings of PANI. A broad peak at 1195 and 1205 cm^{-1} is related to C-N stretching, while the peaks at 3428, 3465, and 3470 cm^{-1} are corresponded to the N-H stretching mode. The FT-IR results indicate that the PANI and

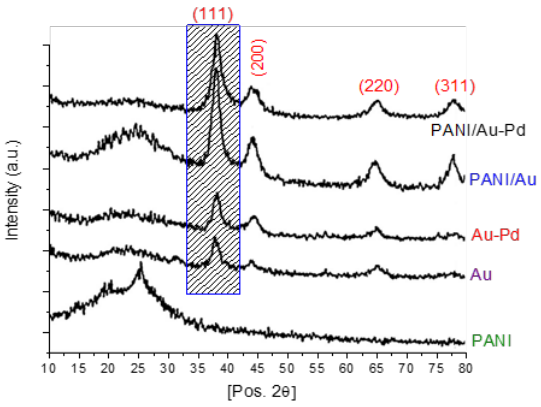

Fig. 3. XRD of PANI, Au, Au-Pd, Au/PANI, and Au-Pd/PANI

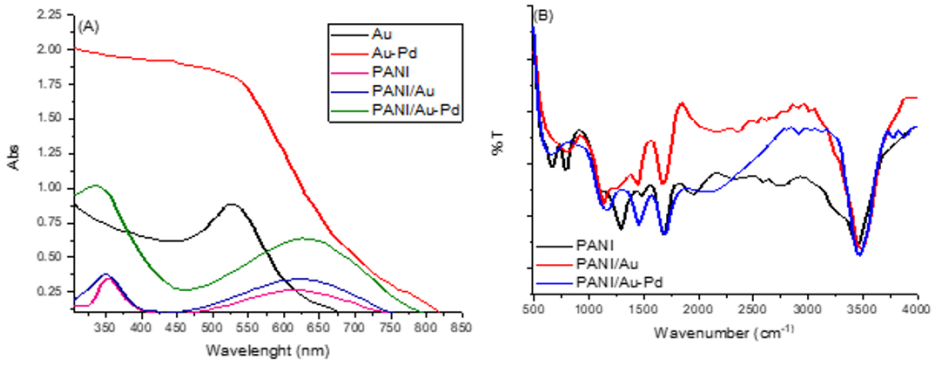

Fig. 2 (A) UV-Vis of Au, Au-Pd, and Au-Pd/PANI, (B) FT-IR of PANI, Au-PANI, and Au-Pd/PANI

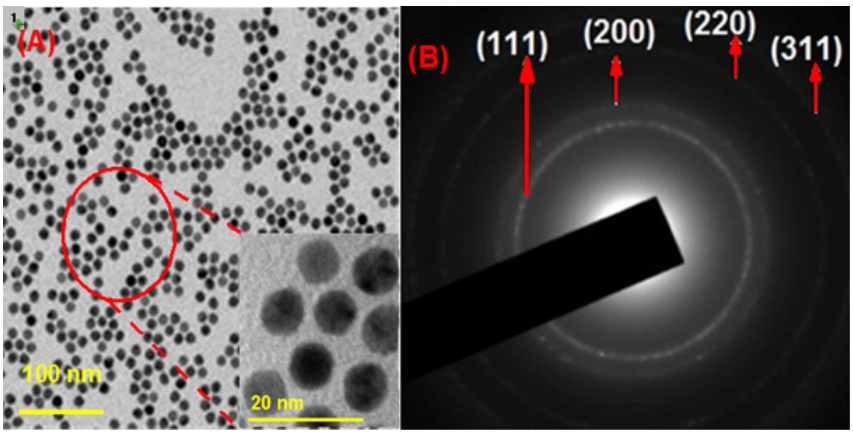

Fig. 4 (A) HRTEM of Au, (B) SAED of Au

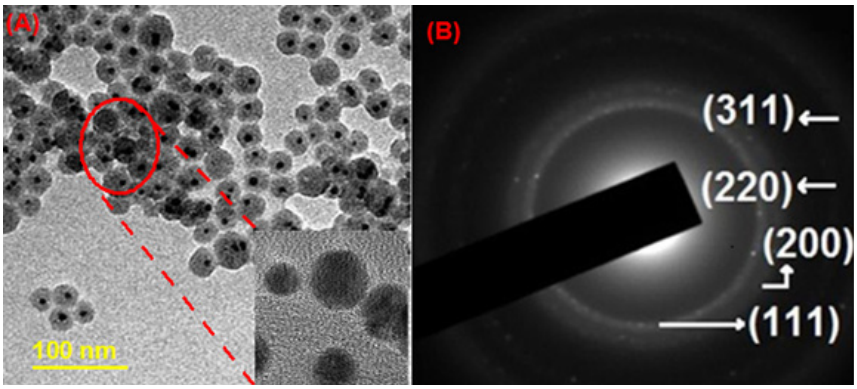

Fig. 5 (A) HRTEM of Au-Pd, (B) SAED of Au-Pd.

its composite are produced in the reaction between aniline monomer and Au and Au-Pd colloidal by using oxidative polymerization [38, 39].

The XRD analysis of PANI, Au, Au-Pd, Au/PANI, and Au-Pd/PANI are shown in Fig.3. For PANI, the results appeared two diffraction peaks located at 20-25o with broader and low intensity, assigned to the periodicity parallel to PANI polymer chains and an amorphous nature. For Au-Pd, the results demonstrate three diffraction peaks located at 38.5, 44.1, and 65.45o, corresponding to (111), (200), and (220) planes. For Au/PANI and Au-Pd/PANI nanocomposite, the XRD analysis shows four diffraction peaks centered at 38.1, 44.3, 65.4, and 78.3, assigned to (111), (200), (220), and (311) planes, related to Au and Au-Pd in PANI as is in agreement with (JCPDS 89-3697) [40]. The results appeared that when the Au or Au-Pd concentration increased, the intensity of the peaks was boosted. It can be deduced that the Au/PANI and Au-Pd/PANI are more crystalline nature than PANI.

The Morphology, lattice fringes, and crystal plane of Au, Au-Pd core shell, PANI, Au/PANI, and Au-Pd/PANI were investigated by HRTEM analysis. For Au nanoparticles (Fig. 4A), the TEM image shows spherical morphology, as well as, it appears a single nanoparticles with fringes spacing of 0.25 nm, corresponding to (111) plane. The SAED results obviously marks the existence of Au NPs, and (111), (200), (220), and (311) planes are in agreement with Au nanoparticles (Fig. 4B).

The HR-TEM images of Au-Pd core-shell nanocomposite are displayed in Fig. (5a,b). The results appeared that the morphology is nearly spherical (Fig. 5a). Besides, it exhibited the single Au-Pd nanoparticles with fringes spacing of 0.25 nm, which suggests the inter-fringe distance of (111) plane. The SAED results of Au-Pd were proven via the (111), (200), (220), and (311) planes (Fig. 5b).

PANI nanotubes seem as a short rods with the diameter of 300-400 nm particularly twisted with each other, perhaps because of the presence of NH groups on the surface. TEM images disclose that the PANI nanotube are hollow or blank from inside, making the tubular structure with an indoor

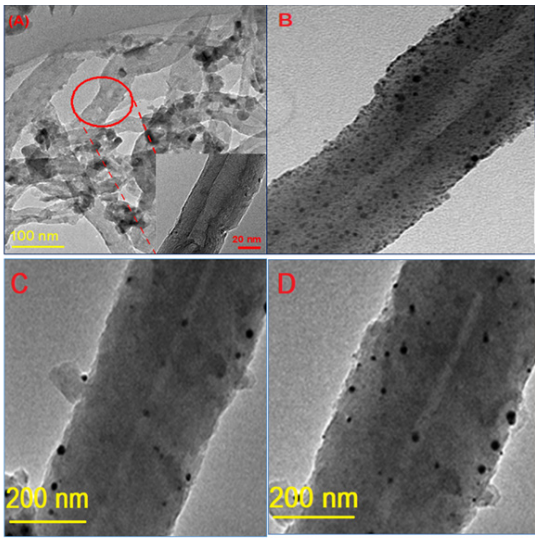

Fig. 6. TEM of (A) PANI, (B) Au/PANI, (C) Pd/PANI, (D) Au-Pd/PANI

diameter of 350-400 nm (Fig. 6). However, it is substantial to remind that most of the ends of PANI nanotubes are sealed, which may be back to the high power used on the system of reaction during irradiation of ultrasonic. Then, the as-synthesized PANI nanotubes were employed as props for the Au-Pd nanoparticles by using hydrazine as a reduce material. The PANI nanotubes incorporated with Au-Pd bimetallic were investigated TEM as shown in Fig. 6A-D. The results demonstrated that the diameter of Cu-Ag nanoparticles in the range of 10-20 nm. Au-Pd evenly was dispersed on the outer wall of PANI nanotubes and didn't alter the PANI morphology. Besides, any aggregation through hydrazine co-reduction on the PANI nanotube indicated the prepared nanotube with affluent OH groups; and these supplies many sites for coordination with Au-Pd bimetallic [41].

Electrochemical characterization

Electrochemical demeanors of DA and HQ were investigated utilizing CV and DPV, as displayed in Fig. 7. Notably, both DA and HQ appeared discrete redox peaks on the Au-Pd/PANI electrode, with considerably improved peak currents compared to GCE, as shown in Fig. 7A,B. DA exhibited no discrete peaks on bare GCE, while HQ showed a broad peak in the CV measurements. Fig. 7A displays that the

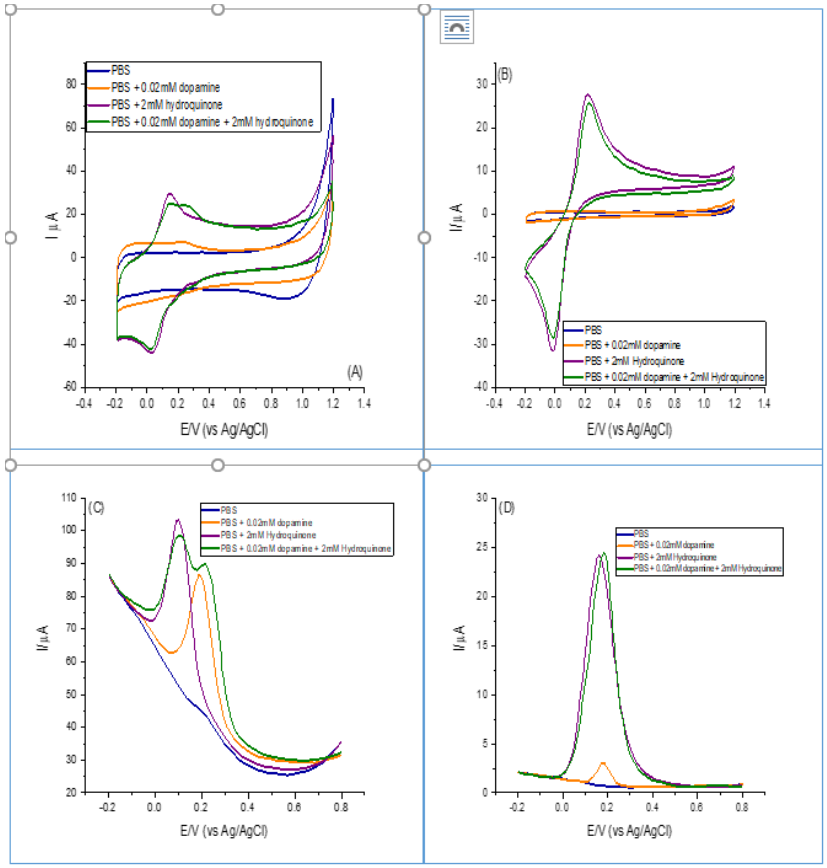

Fig. 7. CV curves of Au-Pd/PANI (A) bare GCE, (B) in (0.01 M, pH 7) PBS at 50 mV/s scan rate, along with the DPV curves for Au-Pd@ PANI (C) bare GCE, (D) in (0.01M, pH 7) PBS

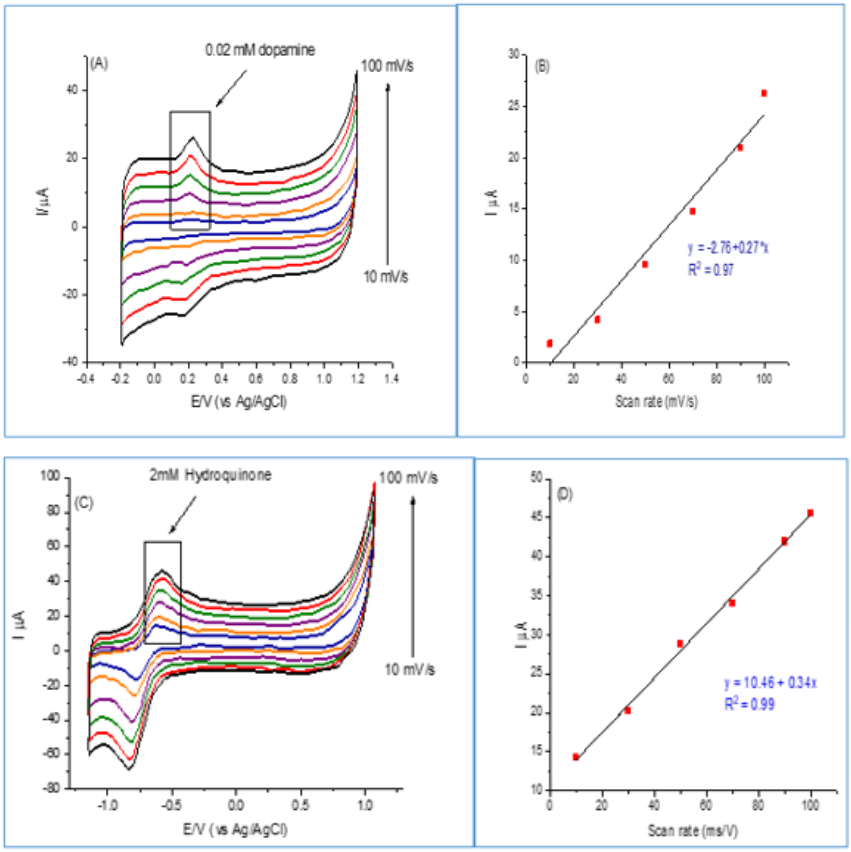

Fig. 8 CV of (A,C) DA and HQ on Au-Pd/PANI in 0.1M PBS, (B,D) Correlation relationship between redox peak and scan rate for DA and HQ

electrochemical reaction of DA and HQ on the Au-Pd/PANI is considerably improved with a higher current of oxidation peak, compared to GCE. The oxidation peak of DA appeared at 196 mV, while a sharp oxidation peak centered at 100 mV. It highlights the reversible anchoring of HQ on Au-Pd/PANI. As a result, the transport of electron on the Au-Pd/PANI electrode is more efficient than bare GCE, thereby Au-Pd can expedite the transfer of electrons. In addition, the 96 mV separation between DA and HQ oxidation could appear good selectivity and reversibility of Au-Pd/PANI electrode for determination of the targets [42]. The DPV results indicate (Fig. 7C,D) overlapping reduction peak of HQ and DA, appearing their uniqueness defying. The electrochemical actions clarified the excellent conductivity and large electrochemically energetic surface area of Au-Pd/PANI electrode.

By studying the kinetics of electrode, the scan rate impact on the Au-Pd/PANI modified electrode gives important premeditations. Total CV analysis in 0.2 M phosphate buffer solution appeared that the currents of the peak redox for DA and HQ increasde with scan rates expanding 10-100 mV/S, as shown in Fig. 8A,C. The results exhibited a linear relationship via the two equation ip = 2.76+0.27*v (R2 = 0.97) and 10.64+0.34*v (R2 = 0.99) assigned to DA and HQ, respectively (Fig. 8B,D). These results propose that the electrochemical interaction of DA and HQ on the Au-Pd/PANI modified surface is related to the model of adsorption-controlled, in agreements with the previous study [43].

Electro-determination of DA and HQ on Au-Pd/PANI electrode

DPV measurements provide more sensitivity and selectivity compared to the CV ones as displayed in Fig. 9A,C. By utilizing DPV, we estimated a broad range of DA and HQ concentration in the range of 5-25 µM and 0.5-2.5 mM, respectively, in incrementally boosting batches. As shown in Fig 9. B,D, a linear relationship was noted between the current of the oxidation peak and concentration of DA and HQ via the following equations of i (10-6A) = 1.88 + 30.4*c (R^2 = 0.98) and 42.08 + 70.24 *c (R^2 = 0.99) [44].

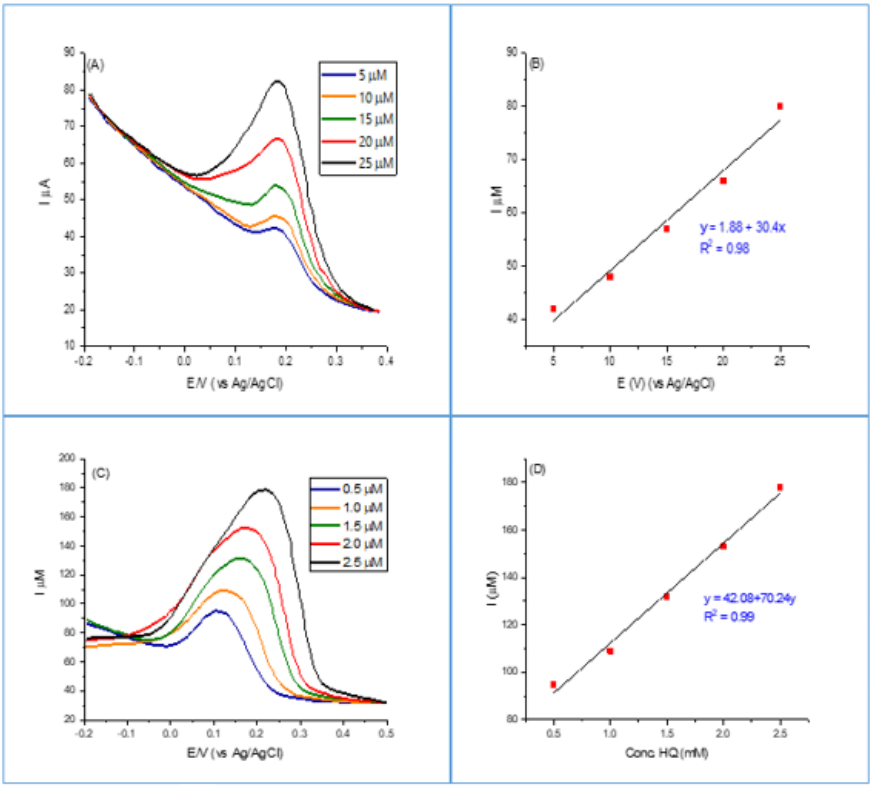

Fig. 9 DPV response of (A,C) DA and HQ on Au-Pd/PANI electrode with (B,D) the related calibration curves

Simultaneous determination of DA and HQ using Au-Pd/PANI electrode

The calibration carves and detection limits for simultaneous sensing of DA and HQ by Au-Pd/PANI electrode were initiated by using DPV measurements in 0.1 M PBS. The response of DPV for DA demonstrated a linear relationship in the range of 2-40 mm. The results (Fig. 10B) showed a linear equation as I (10-6A) = 2.77 + 34.3x (R^2 = 0.99) and 2.40 + 51.04x (R^2 = 0.98). The DPV response for HQ illustrated a linear relationship in the same concentration of DA ($1*10^{-5}$ M) in the range of 0.2-2.5 µM with the equation of i (10-6 A) = 28.69 + 88.11x (R^2 = 0.98) (0.002M) (Fig. 10C,D). These results proposed that the Au-Pd/PANI modified electrode can be efficiently used for the simultaneous determination of DA and HQ.

Stability of electrochemical sensor

To evaluate the Au-Pd/PANI electrode reproducibility, five electrodes were prepared utilizing a proportionate method and experimented for determining DA and HQ. The restraint currents appeared minor inconstancies, with RSD of 1.54% for DA and 2.45% for HQ, indicating the good reproducibility. Moreover, the measurements of CV were carried out over 20 cycles in 0.2M PBS containing 20 µM of DA and 0.002M of HQ. Notably, the current of the redox peaks for DA and HQ stayed stable with final cycle remaining over 98% for the initial value of the peak current, certifying to the Au-Pd/PANI sensor precision.

Real sample analysis

The analysis in real samples was included two stages: the first one contained the electro-determination of DA by Au-Pd/PANI electrode in the DA hydrochloride injection sample. The drug solution (Concentration of 200 mg/mL, 5 mL per injection) was diluted to 10 mL. Then, 1 mL of diluted solution was transferred to 5 mL volumetric flasks series and completed the volume by PBS solution. Finally, 2 mL of the solution was put in the electrochemical cell for investigation of DA via the DPV method, and the results are summarized in Table. 1. The second stage was the electro-determination of DA by Au-Pd@PANI electrode in the human blood serum. By using Au-Pd/PANI sensor, it clarified that the human blood serum was free of DA. However, when the DA

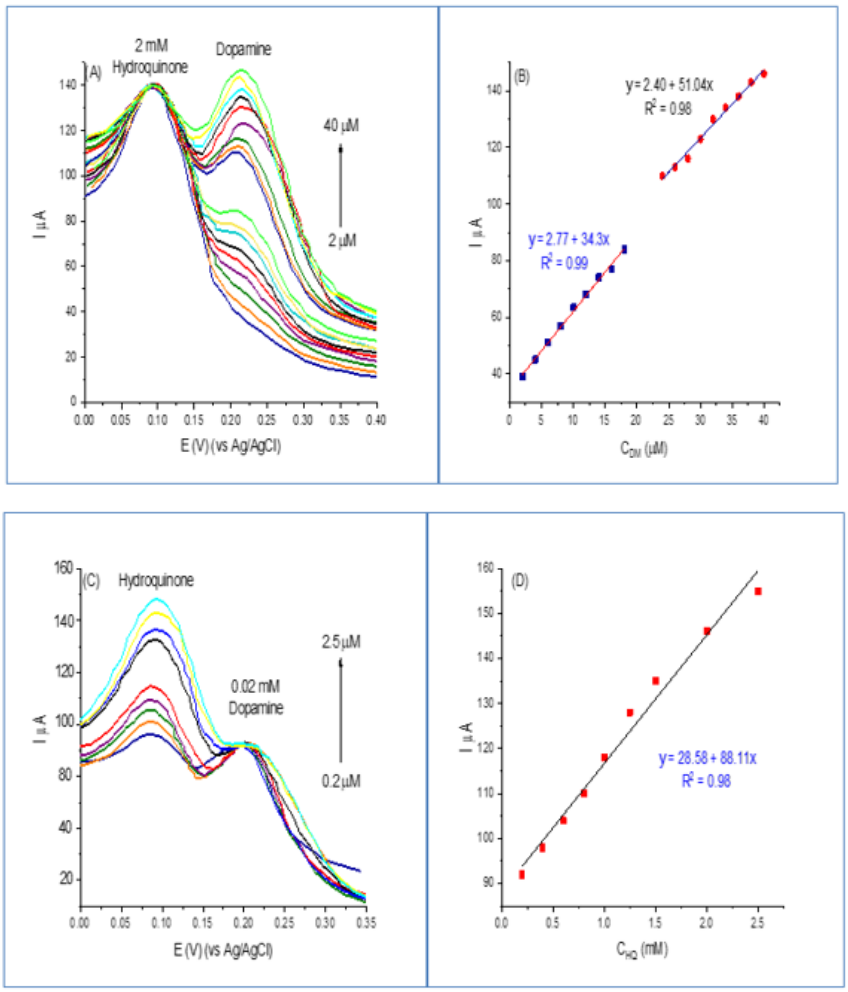

Fig. 10. DVP curve of Au-Pd/PANI electrode for (A,C) 20-40 µM of DA and 0.2-2.5 µM of HQ and (B,D) linear oxidation peak current-DA and HQ conc. relationship

standard solution was spiked, the existence of uric acid and some other meddlesome materials, like glucose and albumin, didn't intervene with the DA determination (Table 1). Au-Pd/PANI reacts good for the spiked DA recovery with high selectivity and sensitivity in rapprochement to other studied methods. This meansthe auspicious properties of Au-Pd@PANI for the sensitive and selective determination of DA in the real samples.

Table 1. DA determination in DA (HCl) and real samples

DA determination in DA (HCl) injection				DA determination in real samples			
Content (mg/ml)	Add (mg/mL)	Found (mg/mL)	Recovery (%)	Samples	Add (µM/L)	Found (µM/L)	Recovery (%)
	0	9.90	-				
	0.3	10.23	97	1	0.2	0.23	99
10	0.6	10.56	96.2				
	0.9	11.24	100.3				
	1.2	11.44	97.1				
	0	9.94	-	2	0.4	0.38	94
	0.3	10.31	94				
10	0.6	10.64	90.2				
	0.9	11.29	95.2	3	0.6	0.55	91
	1.2	11.37	91.6				

CONCLUSION

In this study, bimetallic Au-Pd doped PANI nanocomposite (Au-Pd/PANI) was successfully prepared by the reduction method. The electrochemical investigation illustrated that the Au-Pd/PANI electrode showed good electro-oxidation effectively toward DA and HQ, which can be adjusted as an electrochemical sensor for same materials disclosure at same time. The low detection limits of DA and HQ with broad linear ranges was achieved by the as-suggested electrode.

FUNDING

The authors received no financial support for the publication of this article.

CONFLICT OF INTERSET

The authors declare no conflict of interest.

REFERENCES

1. Klein MO, Battagello DS, Cardoso AR, David NH, Jackson CB, Ricardo GC. Dopamine: Functions, Signaling, and Association with Neurological Diseases. Cell Mol Neurobiol. 2019;39:31–59.
2. Shaikshavali P, Madhusudana R.T, Venu G.T. Development of carbon-based nanocomposite biosensor platform for the simultaneous detection of catechol and hydroquinone in local tap water. J Mater Sci: Mater Electron. 2021;32:5243–5258.
3. Pang Y, Zeng G, Tang L. Laccase biosensor using magnetic multiwalled carbon nanotubes and chitosan/silica hybrid membrane modified magnetic carbon paste electrode. J. Cent. South Univ. Technol. 2011;18: 1849–1856.
4. Singh S.U, Chatterjee S, Lone, SA. Advanced wearable biosensors for the detection of body fluids and exhaled breath by graphene. Microchim Acta. 2022;189:236.
5. Adam H, Gopinath S.C.B, Arshad M.K. An update on pathogenesis and clinical scenario for Parkinson's disease: diagnosis and treatment. Biotech. 2023;13:142.
6. Baranowska, I, Płonka J. Simultaneous Determination of Biogenic Amines and Methylxanthines in Foodstuff—Sample Preparation with HPLC-DAD-FL Analysis. Food Anal. Methods. 2015;8:963–972.
7. Lu L, Zhou Y, Zheng T. SERS and EC dual-mode detection for dopamine based on WO3-SnO2 nanoflake arrays. Nano Res. 2023;16:4049–4054.
8. Hwang E, Lee B. Synthesis of a fluorescence sensor based on carbon quantum dots for detection of bisphenol A in aqueous solution. Korean J. Chem. Eng. 2022;39:1324–1332.
9. Zhang Y, Liu W, Yao W. An electrochemical sensor based on carbon composites derived from bisbenzimidazole biphenyl coordination polymers for dihydroxybenzene isomers detection. Microchim Acta. 2024;191, 20.
10. Zhang J, Hou C, Huang H, Zhang L, Jiang Z, Chen G, Jia Y, Kuang Q, Xie Z, Zheng L. Surfactant-Concentration Dependent Shape Evolution of Au-Pd Alloy Nanocrystals from Rhombic Dodecahedron to Trisoctahedron and Hexoctahedron. Small. 2013;9:538–544.
11. Ye W, Yu J, Zhou Y, Gao D, Wang D, Wang C, Xue D. Green synthesis of Pt–Au dendrimer-like nanoparticles supported on polydopamine-functionalized graphene and their high performance toward 4-nitrophenol reduction. Appl. Catal., B. 2016;181:371–378.
12. Arora N, Mehta A, Mishra A, Basu S. 4-Nitrophenol reduction catalysed by Au-Ag bimetallic nanoparticles supported on LDH: Homogeneous vs. heterogeneous catalysis. Appl. Clay Sci. 2018;151:1–9.
13. Jiang F, Li R, Cai J, Xu W, Cao A, Chen D, Zhang X, Wang C, Shu C. Ultrasmall Pd/Au bimetallic nanocrystals embedded in hydrogen-bonded supramolecular structures: facile synthesis and catalytic activities in the reduction of 4-nitrophenol. J.Mater. Chem. A. 2015;3: 19433−19438.
14. Noor SA, Chou-Yi H, Zaid HM, Hamidreza S, Ehsan K. A graphene oxide/polyaniline nanocomposite biosensor: Synthesis, characterization, and electrochemical detection of bilirubin, RSC Adv. 2023;13:36280-36292.
15. Ekhlas AA, Zaid HM, Anees AK. Sunlight assisted photocatalytic mineralization of organic pollutants over rGO impregnated TiO2 nanocomposite: Theoretical and experimental study. Case Stud. Chem. Environ. Eng. 2023;8: 100446.
16. Chou-Yi H, Zaid HM, Sherzod A, Bahira AM, Usama SA, Murtadha LS, Ghassan FS. Nanocomposites based on Resole/graphene/carbon fibers: a review study. Case Stud. Chem. Environ. Eng. 2023;8:100535.
17. Raya I, Kzar H.H, Mahmoud, ZH, Alim AA, Aygul ZI, Ehsan K. A review of gas sensors based on carbon nanomaterial. Carbon Lett. 2022;32:339–364.
18. Ashkan B, Mahmoud K, Zaid HM, Dmitry B, Baadal JJ, Ali F. Quick and sensitive colorimetric detection of amino acid with functionalized-silver/copper nanoparticles in the presence of cross linker, and bacteria detection by using DNA-template nanoparticles as peroxidase activity. Spectrochim Acta A Mol Biomol Spectrosc. 2022;268:120636.
19. Zaid HM, RA, Anees AK. The efficacy of samarium loaded titanium dioxide (Sm: TiO2) for enhanced photocatalytic removal of rhodamine B dye in natural sunlight exposure. J. Mol. Struct. 2022;1253:132267.
20. Zaid HM, RA, Anees AK. Synthesis and supercapacitor performance of polyaniline-titanium dioxide-samarium oxide (PANI/TiO2-Sm2O3) nanocomposite. Chem. Pap. 2022;76:1401-1412.
21. Zaid HM, RA, Anees AK. Electron transport in dye-sanitized solar cell with tin-doped titanium dioxide as photoanode materials. J. Mater. Sci.: Mater. Electron. 2022;33:5009-5023.
22. Kavitha M, Zaid HM, Kakarla HK, Petrov AM, Aleksandr L, Pavel I, Angelina OZ, Mohammad S. Application of steinberg model for vibration lifetime evaluation of Sn-Ag-Cu-based solder joints in power semiconductors. IEEE Trans. Compon. Packaging Manuf. Technol. 2021;11:444-450.
23. Indah R, Gunawan W, Zaid HM, Abed JK, Kabanov OV, Yasser FM, Mustafa MK, Trias M, Ismail H, Leila K. Kinetic, isotherm, and thermodynamic studies on Cr (VI) adsorption using cellulose acetate/graphene oxide composite nanofibers. Appl. Phys. A. 2022;128:167.
24. Zaid HM, Omar GH, Ahmed NA, Yehya MA, Usama SA, Ashour HD, Riyam S. Functionalize cobalt ferrite and ferric oxide by nitrogen organic compound with high supercapacitor performance. Results Chem. 2023;5:100936.
25. Zaid HM, Yassine R, Hayder AH, Ayad FA, Yasser FM. Magnetic nanoparticles supported copper nanocomposite:

a highly active nanocatalyst for synthesis of benzothiazoles and polyhydroquinolines. Polycycl aromat comp. 2023;43:3687-3705.
26. Chou-Yi H, Al-Salman HNK, Zaid HM, Rawaa MA, Amir FD. Improvement of the photoelectric dye sensitized solar cell performance using Fe/S–TiO2 nanoparticles as photoanode electrode. Sci. Rep. 2024;14:4931.
27. Faezeh M, Arezo M, Yathrib A, Ausama AA, Ahmed RA, Zaid HM, Ehsan K. An experimental study on absorption and catalytic activity of molybdenum-schiff bases complex immobilized on Tl2O3–SiO2 nanoparticles. Case Stud. Chem. Environ. Eng. 2024;9:100684.
28. Chou-Yi, Al-Salman HNK, Hussein HH, Nizomiddin J, Zaid HM, Saeb JA, Hanan HA, Ahmed AA, Nahed MA, Seitkhan A. Experimental and theoretical study of improved mesoporous titanium dioxide perovskite solar cell: The impact of modification with graphene oxide. Heliyon. 2024;10.
29. sabri A, Kadhim MM, Mahdi RA. Alaa DJ, Zainab TA, Firas MD, Asala SJ, Safa KH, Zaid HM, Farah KA, Hasan K, Ehsan K. Preparing Hybrid Nanocomposites on the Basis of Resole/Graphene/Carbon Fibers for Investigating Mechanical and Thermal Properties. BioNanoSci. 2023;13:983–1011.
30. Qiao J, Wu Y, Zhu C. High-performance carbon nanotube/polyaniline artificial yarn muscles working in biocompatible environments. Nano Res. 2023;16:4143–4151.
31. Mahmoud ZH, AL-Bayati RA, Khadom AA. Synthesis and supercapacitor performance of polyaniline-titanium dioxide-samarium oxide (PANI/TiO2-Sm2O3) nanocomposite. Chem. Pap. 2022;76:1401–1412.
32. Zaid HM, Reem AA, Anees AK. In situ Polymerization of Polyaniline/Samarium Oxide - Anatase Titanium Dioxide (PANI/Sm2O3-TiO2) Nanocomposite: Structure, Thermal and Dielectric Constant Supercapacitor Application Study. J. Oleo Sci. 2022;71(2):311-319.
33. Isaeva IY, Ostaeva GY, Eliseeva EA. The Structure of Nanocomposites with Bimetallic Cu–Ni Nanoparticles Obtained by Chemical Reduction. Crystallogr. Rep. 2022;67:987–995.
34. Wang X, Song H, Ma S, Li M, He G, Xie M, Guo X. Template ion-exchange synthesis of Co-Ni composite hydroxides nanosheets for supercapacitor with unprecedented rate capability. J. Chem. Eng. 2022;432:134319.
35. L. Li, S. Lu, Y. Dai, H. Li, X. Wang, Y. Zhang. Controlled Synthesis of Hierarchical Nanostructured Metal Ferrite Microspheres for Enhanced Electrocatalytic Oxygen Evolution Reaction. A.C.S. Appl, Nano Mater. 2023;6(3): 2184–2192.
36. He Q, Kang X, Fu F, Ren M, Liao F. The Synthesis of rGO/Ni/Co Composite and Electrochemical Determination of Dopamine. J. Inorg. Organomet. Polym Mater. 2020;30:4269–4277.
37. Pruneanu S, Veress E, Marian I. Characterization of polyaniline by cyclic voltammetry and UV-Vis absorption spectroscopy. J Mater Sci. 1999;34: 2733–2739.
38. Massoumi B, Fathalipour S. Ternary Ag/Polyaniline/Au nanocomposites: Preparation, characterization and electrochemical properties. Polym. Sci. Ser. A. 2014;56:373–382.
39. Baoyang L, Congcong L, Yuzhen L, Jingkun X, Guodong L. Conducting polynaphthalenes from 1,1′-binaphthyl and 1,1′-bi-2-naphthol via electropolymerization. Synth. Met. 2011;161(1-2):188-195.
40. Singh L, Singh V. Synthesis of Au@PANI nanocomposites by complexation method and their application as label-free chemo probe for detection of mercury ions. Bull Mater Sci. 2020;43:307.
41. Naim NM, Abdullah H, Hamid AA. Influence of Ag and Pd Contents on the Properties of PANI–Ag–Pd Nanocomposite Thin Films and Its Performance as Electrochemical Sensor for E. coli Detection. Electron. Mater. Lett. 2019;15:70–79.
42. Jonke AP, Josowicz M. Janata J. Polyaniline Electrodes Containing Tri-Atomic Au/Pd Clusters: Effect of Ordering. Catal Lett. 2013;143:1261–1265.
43. Rumi A, Sayan DD, Tejal VP, Keya G, Aayushi R, Ki-Taek L. A Review on Electroactive Polymer–Metal Composites: Development and Applications for Tissue Regeneration. J. Funct. Biomater. 2023, 14(10): 523.
44. Sadeghi S, Fooladi E, Malekaneh, MA. New Amperometric Biosensor Based on Fe_3O_4/Polyaniline/Laccase/Chitosan Biocomposite-Modified Carbon Paste Electrode for Determination of Catechol in Tea Leaves. Appl Biochem Biotechnol. 2015;175:1603–1616.